Chin. Geogra. Sci. 2020 Vol. 30 No. 5 pp. 855–875
https://doi.org/10.1007/s11769-020-1151-y

Springer Science Press
www.springerlink.com/content/1002-0063

Evaluating Spatial Heterogeneity of Land Surface Hydrothermal Conditions in the Heihe River Basin

ZHANG Yuan[1], LIU Shaomin[1], HU Xiao[1], WANG Jianghao[2], LI Xiang[1], XU Ziwei[1], MA Yanfei[3], LIU Rui[1], XU Tongren[1], YANG Xiaofan[1]

(1. *State Key Laboratory of Earth Surface Processes and Resource Ecology*, *Faculty of Geographical Science*, *Beijing Normal University*, *Beijing* 100875, *China*; 2. *State Key Laboratory of Resources and Environmental Information Systems*, *Institute of Geographic Sciences and Natural Resources Research*, *Chinese Academy of Sciences*, *Beijing* 100101, *China*; 3. *Department of Geography*, *Handan College*, *Hebei* 056005, *China*)

Abstract: Land surface hydrothermal conditions (LSHCs) reflect land surface moisture and heat conditions, and play an important role in energy and water cycles in soil-plant-atmosphere continuum. Based on comparison of four evaluation methods (namely, the classic statistical method, geostatistical method, information theory method, and fractal method), this study proposed a new scheme for evaluating the spatial heterogeneity of LSHCs. This scheme incorporates diverse remotely sensed surface parameters, e.g., leaf area index-LAI, the normalized difference vegetation index-NDVI, net radiation-Rn, and land surface temperature-LST. The LSHCs can be classified into three categories, namely homogeneous, moderately heterogeneous and highly heterogeneous based on the remotely sensed LAI data with a 30 m spatial resolution and the combination of normalized information entropy (S') and coefficient of variation (CV). Based on the evaluation scheme, the spatial heterogeneity of land surface hydrothermal conditions at six typical flux observation stations in the Heihe River Basin during the vegetation growing season were evaluated. The evaluation results were consistent with the land surface type characteristics exhibited by Google Earth imagery and spatial heterogeneity assessed by high resolution remote sensing evapotranspiration data. Impact factors such as precipitation and irrigation events, spatial resolutions of remote sensing data, heterogeneity in the vertical direction, topography and sparse vegetation could also affect the evaluation results. For instance, short-term changes (precipitation and irrigation events) in the spatial heterogeneity of LSHCs can be diagnosed by energy factors, while long-term changes can be indicated by vegetation factors. The spatial heterogeneity of LSHCs decreases when decreasing the spatial resolution of remote sensing data. The proposed evaluation scheme would be useful for the quantification of spatial heterogeneity of LSHCs over flux observation stations toward the global scale, and also contribute to the improvement of the accuracy of estimation and validation for remotely sensed (or model simulated) evapotranspiration.

Keywords: land surface hydrothermal conditions (LSHCs); evapotranspiration; spatial heterogeneity; remote sensing; evaluation scheme

Citation: ZHANG Yuan, LIU Shaomin, HU Xiao, WANG Jianghao, LI Xiang, XU Ziwei, MA Yanfei, LIU Rui, XU Tongren, YANG Xiaofan, 2020. Evaluating Spatial Heterogeneity of Land Surface Hydrothermal Conditions in the Heihe River Basin. *Chinese Geographical Science*, 30(5): 855–875. https://doi.org/10.1007/s11769-020-1151-y

Received date: 2020-01-20; accepted date: 2020-05-04

Foundation item: Under the auspices of National Natural Science Foundation of China (No. 41531174), National Basic Research Program of China (No. 2015CB953702)

Corresponding author: LIU Shaomin. E-mail: smliu@bnu.edu.cn

© Science Press, Northeast Institute of Geography and Agroecology, CAS and Springer-Verlag GmbH Germany, part of Springer Nature 2020

1 Introduction

Land surface hydrothermal conditions (LSHCs) can reflect land surface moisture and heat conditions, and play an important role in energy and water cycles in soil-plant-atmosphere continuum (Bhattacharya et al., 2010; Nakayama et al., 2013; Gao et al., 2015; Han et al., 2018; Ma et al., 2019; Wang et al., 2019). LSHCs and evapotranspiration (ET) are both controlled by meteorological, soil and vegetation factors, so the change of LSHCs can affect ET, and the change of ET can also reflect LSHCs. The spatial heterogeneity of LSHCs result from the spatial distribution of meteorological (e.g., net radiation (Rn)), soil (e.g., soil moisture (SM)) and vegetation (e.g., leaf area index (LAI), normalized vegetation index (NDVI)) factor, which can bring uncertainty to parameterization schemes of remotely sensed (or model simulated) ET and then affect the accurate estimation of ET at the regional scale (Zhang et al., 2016). Moreover, the spatial heterogeneity of LSHCs also have impact on the spatial representation of in situ observation, and then affect the validation of remotely sensed (or model simulated) ET (Li et al., 2018a). If the spatial heterogeneity of LSHCs is homogeneous, remotely sensed (or model simulated) ET can be validated directly by in situ observation. If the spatial heterogeneity of LSHCs is heterogeneous, there is a spatial scale mismatch between them, which brings uncertainty to validation process (Wu et al., 2019). Because remotely sensed (or model simulated) ET arranged in pixels (or grids), while the source area of flux ground measurements varies with the height of the instrument, wind speed/direction, atmospheric stability and surface roughness (Li et al., 2018a). In order to improve the reliability of validation, based on the spatial heterogeneity of LSHCs to choose appropriate upscaling methods to get ground truth ET at pixel scale is very important (Liu et al., 2016; Li et al., 2018a). Therefore, it is vital to study the spatial heterogeneity of LSHCs to support the accurate observation of ET and the validation of ET remote sensing estimation and model simulation.

Various methods have been applied to quantitatively evaluate the spatial heterogeneity of LSHCs. These methods include but are not limited to the classic statistical method (Garrigues et al., 2006), geostatistical method (Cressie, 1992), information theory method (Shannon, 1948), and fractal dimension method (Clarke, 1986). The topography, land cover type, soil type and moisture, vegetation type and growth status, radiation and precipitation are complex and interactive, which result from the spatial heterogeneity of LSHCs. The land surface temperature (LST) can directly reflect the moisture and heat conditions of the land surface. The spatial distribution and variation of vegetation are determined by the land surface hydrothermal conditions. Most of previous studies focused on the evaluation of the LSHCs (Ding et al., 2014; Hu et al., 2015; Xu et al., 2016). However, specific studies on the evaluation schemes for the heterogeneity of LSHCs are still rare, including those using single method or factor to characterize the spatial heterogeneity of LSHCs (Ding et al., 2014; Hu et al., 2015; Xu et al., 2016). For instance, Hu et al. (2015) analyzed the spatial heterogeneity of LSTs based on the Thermal Airborne Hyperspectral Imager (TASI) and Advanced Spaceborne Thermal Emission Reflection (ASTER) data with the geostatistical method. The results showed that the spatial heterogeneity of LSTs increased with spatial scale until the scale was larger than the characteristic scale, and the land cover types can significantly influence the spatial heterogeneity of LSTs. Ding et al. (2014) quantified the spatial heterogeneity of cropland using the varigorams of multi-temporal NDVI. They found the NDVI shows the greatest heterogeneity in the early stage of crop growth. With an increase in the image pixel size, the spatial heterogeneity quantified by the mean variability of the NDVI tends to be the same. ET plays a crucial role in the surface hydrothermal balance (Nakayama, 2013; Kong et al., 2019), many studies have carried out to discussed the spatial heterogeneity of ET (Alfieri et al., 2009; Giannico et al., 2018; Li et al., 2018a; 2018b). For example, Li et al. (2018a) used the coefficient of variation (*CV*) as the evaluation index based on the eddy covariance (EC) system in the midstream and downstream regions of Heihe River Basin (HRB) to evaluate the spatial heterogeneity of ET. The results showed that the spatial heterogeneity of ET at midstream during the crop growing period was relatively small and vulnerable to irrigation and rainfall. The spatial heterogeneity of ET downstream was greater than that at midstream. It is well known that vegetation and energy factors influence ET (Gao et al., 2006). The changes in these factors can indirectly express the spatial-temporal variation in ET (Li and Avissar, 1994).

Therefore, the spatial heterogeneity of ET can be indirectly characterized by the spatial heterogeneities of these parameters. For instance, Li and Avissar (1994) compared the effects of five surface parameters (stomatal conductance, SM, LAI, surface roughness, and albedo) on the estimation of sensible/latent heat flux. And the results showed that LE is sensitive to spatial distribution of surface parameters, and if considering the spatial variability in the LAI, stomatal conductance and SM in bare soil are also important to the estimation of sensible/latent heat flux.

Progress has been made to describe the spatial heterogeneity of LSHCs by using either some quantitative or semi-quantitative methods. However, there is no quantitative evaluating and grading scheme for the spatial heterogeneity of LSHCs. There is still lack of a unified evaluation method for the spatial heterogeneity of LSHCs of flux stations under different surface types. Moreover, there is no corresponding validation on the evaluation results of spatial heterogeneity of LSHCs, and no detailed analysis on the influencing factors of the evaluation effect of spatial heterogeneity. To overcome the above limitations, a spatial heterogeneity evaluation scheme for LSHCs was proposed in this study. Based on the evaluation scheme, the spatial heterogeneity of LSHCs were evaluated and validated, and the impact factors were discussed. Our study was motivated by the 'Heihe Water Allied Telemetry Experimental Research-Multi-scale Observation Experiment on Evapotranspiration over Heterogeneous Land Surfaces' (HiWATER-MUSOEXE) experiment (Xu et al., 2013; Liu et al., 2016), which was conducted on the midstream region of the HRB in 2012, and the Heihe Integrated Observatory since 2013 (Liu et al., 2011; Liu et al., 2018b). Thus, the HRB is considered as an ideal place that can provide high spatial resolution satellite remote sensing images (such as images of the LAI, NDVI, LST, Rn and ET) (Ma et al., 2018; Xu et al., 2019) and airborne remote sensing data (Xiao and Wen, 2013). Firstly, the study area, the datasets and the descriptions of the four evaluation methods of spatial heterogeneity are described. Then, the specific evaluation scheme and evaluation results and validation at the flux observation stations are presented. Finally, the impact factors of the heterogeneity evaluation scheme are discussed. The main research objectives of this study are as follows: 1) to propose a spatial heterogeneity evaluation scheme for LSHCs by combining four evaluation methods (the classical statistical method, geostatistical method, information theory method and fractal method) based on assessment factors of LSHCs; 2) to quantitatively evaluate spatial heterogeneity of LSHCs at typical flux observation stations in the HRB, and to validate the evaluation results; and 3) to analysis the factors that influencing the evaluation effect of spatial heterogeneity of LSHCs. The proposed evaluation scheme would be useful for the quantification of spatial heterogeneity of LSHCs over flux observation stations, and also contribute to the improvement of the validation for remotely sensed (or model simulated) evapotranspiration.

2 Materials and Methods

2.1 Study area

The study area is located in the Heihe River Basin (HRB) (97°06′E–102°00′E and 37°42′N–42°00′N). The total area of the HRB is approximately 14.3×10^6 km^2. The HRB is the largest endorheic river in the State's Natural Protective Region of Qilian Mountain and the core region of the Silk Road Economic Belt. The HRB has distinct climate characteristics and land cover types among its upstream, midstream, and downstream regions (Xu et al., 2018). The dominant vegetation type in the upstream of the HRB is subalpine meadow and Qinghai spruce. The midstream of the HRB is characterized by the oasis-desert landscape. The dominant vegetation type in the downstream region is shrub forest, such as *Tamarix* and *Populus euphratica*. In this study, flux observation stations with typical land surface types in Heihe River Basin were selected to analyze the spatial heterogeneity of LSHCs (See Table 1). To improve the observation and data collection for studying watershed eco-hydrological processes, the Heihe Integrated Observatory Network of land surface processes was founded. In 2007, during the 'Watershed Allied Telemetry Experimental Research' experiment (WATER, 2007–2011) (Li et al., 2009), the Heihe Integrated Observatory Network of land surface processes was first established. Then, in 2013, it was completed during 'Heihe Watershed Allied Telemetry Experimental Research' experiment (HiWATER, 2012–2015) (Li et al., 2013). The integrated observatory focuses on 23 observation stations covering the main underlying surfaces in the HRB (Liu et al., 2011; Liu et al., 2018b) (Fig. 1a).

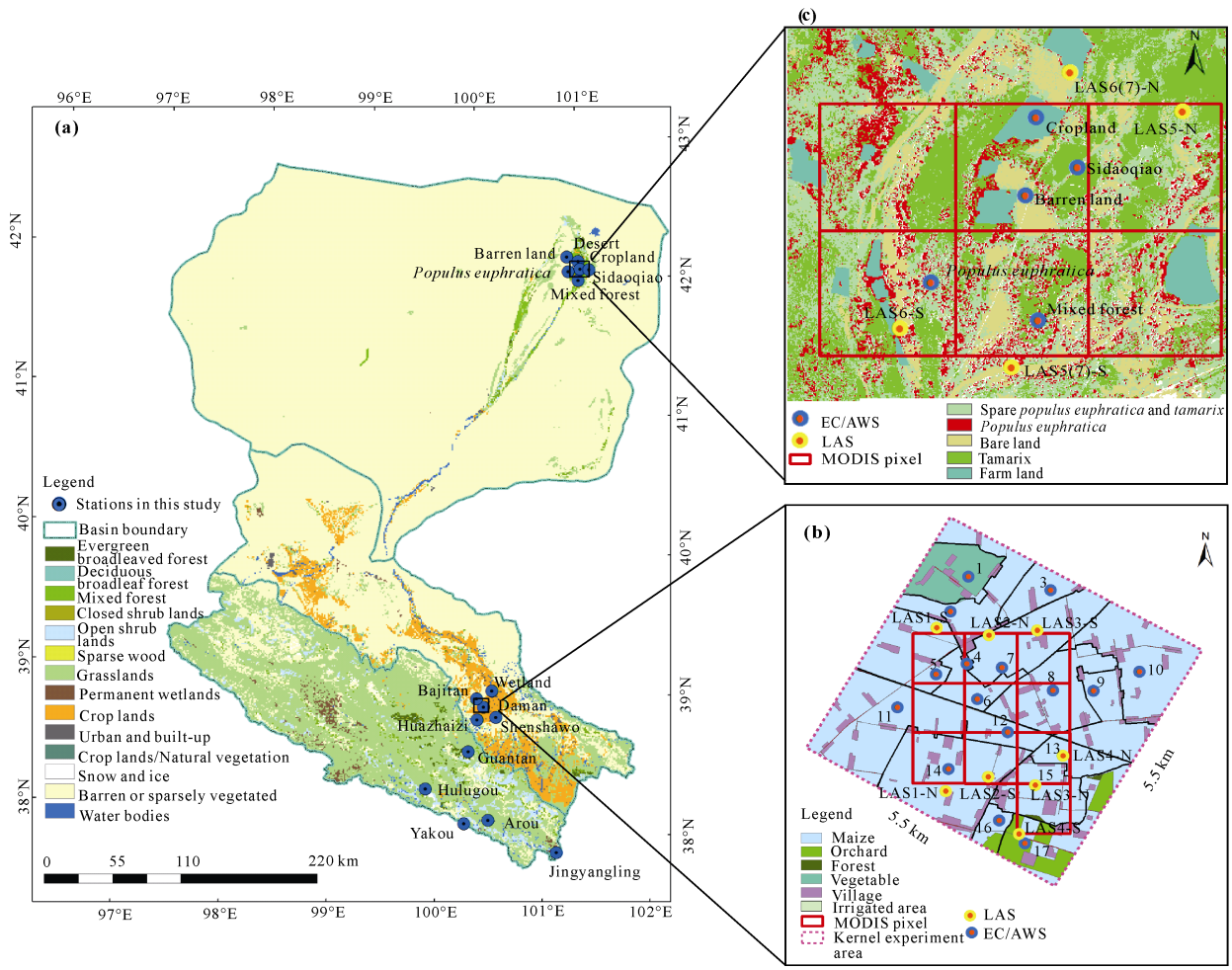

Fig. 1 Land cover types and distribution of flux observation stations in the Heihe River Basin used in this study (a) and the flux observation matrixes in its midstream (b) and downstream regions (c). The land cover map produced based on Zhong et al. (2014)

Currently, the integrated observatory comprises three superstations and eight ordinary stations for long-term operation (Liu et al., 2018b).

There were two flux observation matrixes in the midstream and downstream region of the HRB, which contained intensive observations over various land cover types and high resolution aerial and satellite remote sensing data. Thus, these two regions were takine as the experimental area to select the most suitable evaluation indexes and assessment factors for constructing an appropriate evaluation scheme of the spatial heterogeneity of LSHCs (Fig.1b and Fig. 1c).

From June to September 2012, the thematic experiment HiWATER-MUSOEXE was implemented in the Zhangye oasis-desert area of the midstream region, and two nested matrixes were constructed (Li et al., 2013). The 30 km × 30 km flux observation matrix (the large matrix) consisted of five stations, with one in the oasis (Daman superstation) and four (Wetland station, Bajitan station, Shenshawo station and Huazhaizi station) around the oasis. The 5 km × 5 km flux observation matrix (the kernel matrix located in oasis) (Fig. 1b) was divided into seventeen elementary sampling plots according to the crop structure, trend in forest shelter, distributions of villages and roads, SM and irrigation status (for example, site 1 is the vegetable; the site 4 is the village; the site 17 is the orchard; and other sites is the maize). There was one EC station and one automatic weather station (AWS) in each sampling plot. Moreover, four groups of large aperture scintillators (LASs) were installed at the center of the midstream matrix, three groups of optical LASs were installed in three 3 × 1 MODIS pixels, and another group covered a 2 × 1 MODIS pixel. A wireless sensor network (WSN) that

measures soil temperature, SM, and LAI was set up in the kernel matrix area to accurately measure the parameters of the ET assessment factors in the whole matrix area and each plot. During the HiWATER experiment, airborne remote sensing experiments were successively carried out in the midstream of the HRB. There were a total of 45 missions (approximately 210 flight hours for the airborne remote sensing experiments), which provided high precision underlying surface information. Detailed information on the observation sites and instruments can refer to Liu et al. (2016) and Li et al. (2018a).

Moreover, five stations were located in a 2 km × 3 km flux observation matrix in the downstream oasis (Fig. 1c), including the Sidaoqiao superstation, Cropland station, mixed forest station, Bare land station, and *Populus euphratica* station. There were one EC station and one AWS in each station. Two groups of LASs were set up in the flux observation matrix during July 2013 to May 2015 and then adjusted to a group of LAS (Li et al., 2018a) after May 2015. In addition, the Airborne Light Detection And Ranging (LiDAR), Charge-Coupled Device (CCD) and thermal imager were utilized in the core area of the Ejina Banner oasis in the downstream region. Information about the observation instruments and underlying surfaces in the flux matrix can be found in references Li et al. (2009), Liu et al. (2016) and Li et al. (2018a).

2.2 Datasets

2.2.1 Ground observation data

The sampling frequency of the EC data was 10 Hz, which was processed using Eddypro (https://www.bgc-jena.mpg.de/REddyProc/brew/REddyProc.rhtml). Processing mainly included spike detection, coordinate rotation, sonic virtual temperature correction, density fluctuation correction, and frequency response correction. A quality assessment for the processed 30-min data was performed, including a stationarity test and integral turbulence characteristics test. To obtain the daily ET, the missing data were filled by a nonlinear regression method (Liu et al., 2011; Xu et al., 2013), and the bowen ratio closure method was used to force energy balance closure (Twine et al., 2000). In this study, the EC data from June to September 2012 in the midstream flux observation matrix (3 × 3 MODIS pixels) and downstream flux observation matrix (2 × 3 MODIS pixels) during 2014–2015 were used. The flux observatory stations used in this study are in Table 1.

Table 1 Detailed information of flux observatory stations used in this study

Region	Station name	Vegetation type/land cover	Flux observation instrument	Footprint covered MODIS pixels	Duration
Upstream	Arou	Subalpine meadow	EC+LAS	2×1	2008.6–
	Guantan	Qinghai spruce	EC	2×1	2008.1–2011.12
	Yakou	Alpine meadow	EC	1×1	2015.1–
	Hulugou	Alpine meadow and shrub	EC	1×1	2011.9–
	Jingyangling	Alpine meadow	EC	1×1	2018.8–
Midstream	Daman	Maize	EC+LAS	2×1	2012.5–
	Wetland	Reed		1×1	2012.6–
	Bajitan	*Reaumuria* desert	EC	1×1	2012.6–2015.4
	Shenshawo	Sandy desert	EC	1×1	2012.6–2015.4
	Huazhaizi	*Kalidium foliatum* desert	EC	1×1	2012.6–
Downstream	Sidaoqiao	Tamarix	EC+LAS	2×1	2013.7–
	Mixed forest	*Populus euphratica* and *Tamarix*	EC	1×1	2013.7–
	Desert	*Reaumuria* desert	EC	1×1	2015.4–
	Bare land	Bare land	EC	1×1	2013.7–2016.3
	Cropland	Melon	EC	1×1	2013.7–2015.11

Notes: EC refers to the eddy covariances system, LAS refers to the large aperture scintillator and MODIS refers to the Moderate Resolution Imaging Spectroradiometer). Hulugou station in upstream is collected from other researchers (Chen et al., 2014)

The AWSs from the flux observation matrixes in the midstream and downstream regions of the HRB provided precipitation, Rn, and LST data for this study. The AWS data were collected every 30s and processed into a 30 min averaging period. The data processing of the AWS mainly included drawing the graph for each observation element, eliminating the observation data that were obviously beyond the physical meaning, and linear regression interpolation for the missing data (Liu et al., 2016).

The temporal and spatial distributions and dynamic change characteristics of SM and LAI over the heterogeneous surface were important for this study. A total of 50 WATERNET (at depths of 4 and 10 cm), 50 SoilNet (at depths of 4, 10, 20, and 40 cm), and 80 BNUNET (at depths of 4, 10, and 20 cm) nodes were distributed in the kernel matrix area (Jin et al., 2014; Liu et al., 2018b), forming a dense SM on-site measurement network. The LAI on-site measurement data were derived from the LAINet. The LAINet was present in the kernel matrix area. Each sink node was connected to three to nine measurement nodes using the network. A total of 42 measurement nodes under the canopy, and three above the canopy were established to measure the LAI (Qu et al., 2013). It should be noted that, there are 16 notes of soil moisture (at depth of 4 cm) and 15 notes of LAI in the midstream flux observation matrix were used in section 3.1.1 for comparison of spatial heterogeneity evaluation results based on ground observation data and remote sensing data.

2.2.2 Remote sensing data

LAI, NDVI, LST and Rn data were obtained based on the enhanced spatial and temporal adaptive reflectance fusion model (Zhu et al., 2010) by fusing multisource satellite remote sensing data (MODIS and ASTER/ Enhanced Thematic Mapper plus (ETM+)), then resampled to 30 m. These data were of the midstream flux observation matrix region (covered typical stations such as Daman superstation, Wetland station, Bajitan station, Shenshawo station and Huazhaizi station) from June to September 2012 and of the downstream flux observation matrix region (covered typical stations such as Sidaoqiao superstation, mixed forest station, farmland station, bare land station, and *Populus euphratica* station) during 2014–2015.

ET can be used as a reference index of the LSHCs, the spatial resolution of current ET products is mostly ranged from 1 km to 25 km, which impossible to accurately characterize the variation trend of spatial heterogeneity of LSHCs in a medium resolution satellite pixel such as MODIS pixel (1000 m) (Ma et al., 2018). Thus, the high–spatiotemporal–resolution ET is important for the evaluation of spatial heterogeneity of LSHCs. In this study, the high spatiotemporal resolution ET for June to September in (during 2010) in upstream flux observations (the data covered typical stations such as Arou superstation, Guantan station, Yakou station, Hulugou station and Jingyangling station), midstream flux observation matrix (in 2012) and downstream flux observation matrix (during 2014–2015) (the desert station is out of the downstream flux observation matrix region but also provided for this study) were derived from the optimized SEBS model (Ma et al., 2018).

Airborne data were obtained from aerial remote sensing experiments conducted in the midstream matrix region in 2012 and the downstream matrix region in 2014 and include wide-angle infrared dual-mode line/area array scanner (WiDAS) data (Xiao and Wen, 2013), TASI data (Xiao and Wen, 2013), Airborne Light Detection And Ranging data (Boudreault et al., 2015; Liu et al., 2018a), and the inversed polarimetric L-band multibeam radiometer (PLMR) (Li et al., 2017) SM data. These data have been preprocessed (including radiation correction, geometric correction, *etc*.). Information on satellite remote sensing and airborne data is summarized in Table 2. In addition, this study also used Google Earth imagery to provide reference information for land use in MODIS pixels where each station was located.

2.2.3 Footprint data

In this study, MODIS pixels were selected according to the observed flux source area of each station; then, the LSHCs in these MODIS pixels were evaluated. Flux observatories based on the EC system and LAS can continuously measure energy, water, and CO_2 fluxes between the ecosystem and atmosphere. The observed flux source areas of the flux observation stations are different. Usually, the source area of the EC system is usually a few to hundreds of meters, and that of the LAS is approximately 500–5000 m (Jia et al., 2012). The observed flux source area varies with elevation, wind direction/wind speed, atmospheric stability, and surface roughness. Therefore, it is necessary to determine the source area of the observational flux, which refers to the

Table 2 Information of satellite remote sensing and airborne data

Surface parameters	Sensor	Region	Flight duration	Spatial resolution (m)	Reference
LST, LAI	WiDAS	Midstream matrix	August 2, 2012	7.5	(Xiao and Wen, 2013)
LST	TASI	Midstream matrix	June 30, July 10, 2012	3	(Xiao and Wen, 2013)
SM	PLMR	Midstream matrix	June 30, July 7, July 10, July 26, August 2, 2012	700	(Li et al., 2017)
LAD	LiDAR	Midstream matrix; Downstream matrix	July 19, 2012; July 29, 2014	15 20	(Boudreault et al., 2015; Liu et al., 2018a)
LAI \NDVI\Rn\ LST	MODIS/ASTER/ ETM+	Midstream matrix; Downstream matrix/HRB typical stations	June to September, 2012 in midstream; June to September, 2014–2015 in downstream/June to September, 2010 in upstream; June to September, 2012 in midstream; June to September, 2014–2015 in downstream.	30/90/1000	(Ma et al., 2018)
ET	MODIS/ASTER/ ETM+	Midstream matrix; Downstream matrix/HRB typical stations	June to September, 2012 in midstream; June to September, 2014–2015 in downstream/June to September, 2010 in upstream; June to September, 2012 in midstream; June to September, 2014–2015 in downstream.	30	(Ma et al., 2018)

Notes: LST refers to the Land Surface Temperature, LAI refers to the Leaf Area Index, SM refers to the Soil Moisture, LAD refers to the Leaf Area Density, NDVI refers to the Normalized Vegetation Index, Rn refers to the Net Radiation, ET refers to the evapotranspiration, WiDAS refers to Wide-angle Infrared Dual-mode line/Area array Scanner, TASI refers to the Thermal Airborne Hyperspectral Imager, PLMR refers to the Polarimetric L-band Multibeam Radiometer, LiDAR refers to the Airborne Light Detection and Ranging, MODIS refers to the Moderate Resolution Imaging Spectroradiometer, ASTER refers to the Advanced Space-borne Thermal Emission Reflection, ETM+ refers to the Enhanced Thematic Mapper, and HRB refers to the Heihe River Basin

area of the footprint that has a major contribution to the observational flux. In this study, an Eulerian analytic flux footprint model proposed by Kormann and Meixner (2001) was used to calculate the climatological footprint of the EC system in the growing season (select 90% contribution source area). The climatological footprint of the LAS in the growing season can be calculated by combining the path-weighting function of the LAS with the footprint model for point fluxes (select 90% contribution source area) (Meijninger et al., 2002).

2.3 Evaluation methods for spatial heterogeneity of LSHCs

Four methods for quantitative evaluation of spatial heterogeneity were employed. Through the combination of different evaluation methods and assessment factors, the most suitable evaluation methods and assessment factors were selected to construct the evaluation scheme for the spatial heterogeneity of LSHCs. These methods include the classic statistical method (Odongo et al., 2014), geostatistical method (Matheron, 1963), information entropy method (Shannon, 1948), and fractal method (Clarke, 1986). The classic statistical method is the most common mathematical-statistical method. The geostatistical method and information theory method are often used in geography to express spatial heterogeneity. Most of the data in this study were derived from remote sensing images; thus, the fractal method was also employed to analyze the fractal structure.

(1) The *CV* is the evaluation index of the classic statistical method. The *CV* is known as the 'coefficient of variation', a normalized measure to the degree of the probability distribution dispersion. The *CV* is defined as the ratio of the standard deviation to the mean value, which can represent the average relative variability of a dataset (Odongo et al., 2014). The mean value reflects the concentrated trend in data, and the variance is used to measure the degree of deviation between the random variable and the mean value, whose arithmetic square root is called the standard deviation.

$$CV = \frac{\sigma}{\overline{x}} = \frac{\sqrt{\frac{1}{n}\sum_{i=1}^{n}\left(x_i - \overline{x}\right)^2}}{\overline{x}} \tag{1}$$

where σ represents the standard deviation of the data, $\overline{x}$ is the mean value of the data and n represents the number of data samples. The *CV* can reflect the spatial heterogeneity of specific physical quantities to a certain extent. The larger the *CV* is, the higher the spatial heterogeneity of physical quantities.

(2) The geostatistical method can consider the spatial variability in geological variables, namely, spatial autocorrelation and randomness, and can be used as a stochastic function of the reaction regionalization phenomenon as a tool to perform various spatial variability (Matheron, 1963) analyses. The variogram can describe the structural changes and random variation in regionalized variables. It is a key function to study the spatial variability of regionalized variables. The calculation formula is:

$$\gamma(h)=\frac{1}{2N(h)}\sum_{i=1}^{N}\left[Z(sp_i)-Z(sp_i+h)\right]^2 \tag{2}$$

where $\gamma(h)$ is the variogram, h is the distance between the sample points, $N(h)$ is the number of samples with a separation distance h, $Z(sp_i)$ and $Z(sp_i+h)$ are the observations of the regionalized variable $Z(sp_i)$ and $Z(sp_i+h)$ at spatial positions sp_i and sp_i+h, and i is the number of the sample point.

The evaluation index of the geostatistical method is the coefficient of the sill (CS), which can provide an opportunity to compare each spatial heterogeneity for different elements in different phases (Xu et al., 2016). The formula is as follows:

$$CS(s)=\frac{\sqrt{c0(sc)+c(sc)}}{\mu(sc)}\times 100\% \tag{3}$$

where $c0(sc)+c(sc)$ is the sill value and $\mu(sc)$ is the mean value of the high-resolution remote sensing product at the pixel scale sc. The larger the CS is, the greater the spatial heterogeneity of the product.

(3) The information entropy (S) method, also called the Shannon entropy method, is a state variable in thermodynamics that can represent the degree of chaos. Shannon introduced this method into information theory, and now it represents a measure of the heterogeneity of a random variable (Shannon, 1948). In the concept of entropy, a random variable is divided into several intervals, each of which represents a state of the random variable, and entropy is the average measure of all possible states of the random variable. When the random variable has only one state or a single value distribution, its entropy is zero. The larger the value of entropy is, the greater the heterogeneity of the random variable.

$$S=-\sum(P_i\ln P_i) \tag{4}$$

where P_i represents the probability that the random variable falls within the interval i. To allow variables to be compared with each other, the information entropy is normalized as the evaluation index (S'), and the formula is as follows:

$$S'=-\sum(P_i\ln P_i)/\ln m \tag{5}$$

where m represents the total amount of variable.

(4) The fractal method is defined as a shape that is partially similar to the whole area in some way. Fractal analysis is based on fractal geometry and describes geometric shapes with similar structures (Clarke, 1986). Fractal theory, as a powerful tool to explain the dynamic mechanisms of complex systems, has been used in so many fields, such as meteorology, geography, hydrology, physics, and biology (Sun et al., 2006). The fractal dimension (D) is a quantitative description index of spatial heterogeneity from the fractal method. The fractal dimension can be calculated as the evaluation index by the following formula:

$$D=3-T/2 \tag{6}$$

where D represents the fractal dimension and T represents the slope of the curve before the variogram $\gamma(h)$ reaches the sill value.

2.4 Flow chart

In this study, the spatial heterogeneity of LSHCs was estimated and evaluated. However, efforts to retrieve the LSHCs based on ET are frequently frustrated by the need to obtain ET data at high spatial resolutions. Considering the applicability and extensibility, the spatial heterogeneity of LSHCs was evaluated through the optimized assessment factors (LAI, SM, Rn, LST) and evaluation methods (classical statistical method, geostatistical method, information theory method and fractal method). The estimated spatial heterogeneity of LSHCs was validated by Google images and high spatial resolution ET data. The flowchart of this study is shown in Fig. 2. The integration of different evaluation schemes included three steps. Firstly, the evaluation methods for the LSHCs were inter-compared using remote sensing data and ground observation data. Then, the evaluation scheme was proposed through assessment factor analysis and evaluation threshold of the LSHCs determination. Based on the proposed evaluation scheme, the LSHCs were evaluated at typi-

cal flux observation stations in the HRB. The evaluated results were also assessed by Google Earth images and high spatial resolution ET products (It is worth noting that high spatial resolution ET products are only used to verify the heterogeneity evaluation results because they are difficult to obtain). Finally, several impact factors of evaluation scheme of LSHCs were discussed, such as precipitation and irrigation events, spatial resolutions of remote sensing data, heterogeneity in the vertical direction, topography and sparse vegetation.

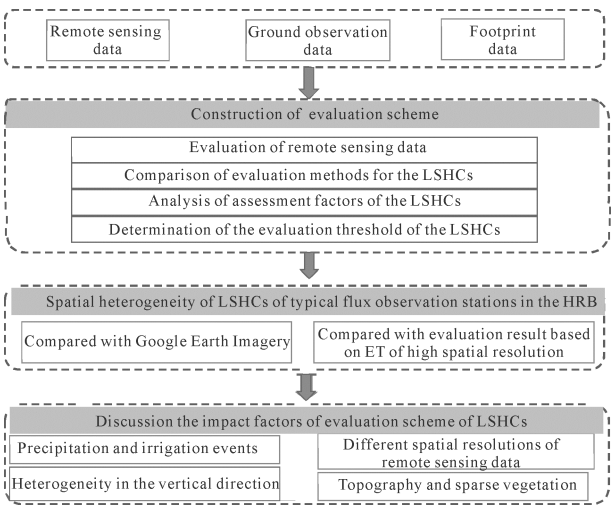

Fig. 2 The flow chart of this study. The LSHCs refers to the Land Surface Hydrothermal Conditions, HRB refers to the Heihe River Basin and ET refers to the evapotranspiration

3 Results

3.1 Construction of evaluation scheme

3.1.1 Evaluation of remote sensing data

Fig. 3 compares the spatial heterogeneity of LSHCs between remote sensing (the circles) and ground observation (the dotted lines) data based on the *CV*. The *CV* values in Fig. 3 were first calculated based on high spatial resolution remote sensing data (LAI, SM, Rn, LST, and ET), and then calculated based on dense multi-site observation data in the same region. As can be seen from Fig. 3b, the spatial resolution of soil moisture data retrieved by aerial remote sensing (PLMR) is relatively coarse (i.e., 700 m), resulting in the difference in the response of soil moisture based on aerial remote sensing (700 m) and ground observation (the average of 16 notes at the depth of 4 cm) to the land surface hydrothermal conditions, especially on July 10. Irrigation occurred on that day, and the change in SM was accurately captured by the site measurements, but the PLMR was hardly able to reflect the change in the spatial heterogeneity of LSHCs at the field scale due to its coarse spatial resolution. The Fig. 3 demonstrated that, remote sensing data can be used to evaluate the spatial heterogeneity of LSHCs except for the PLMR data. In addition, the SM data were relatively coarse (700 m), and the data were only available for five days. The LST can also be taken as the energy factor to reflect

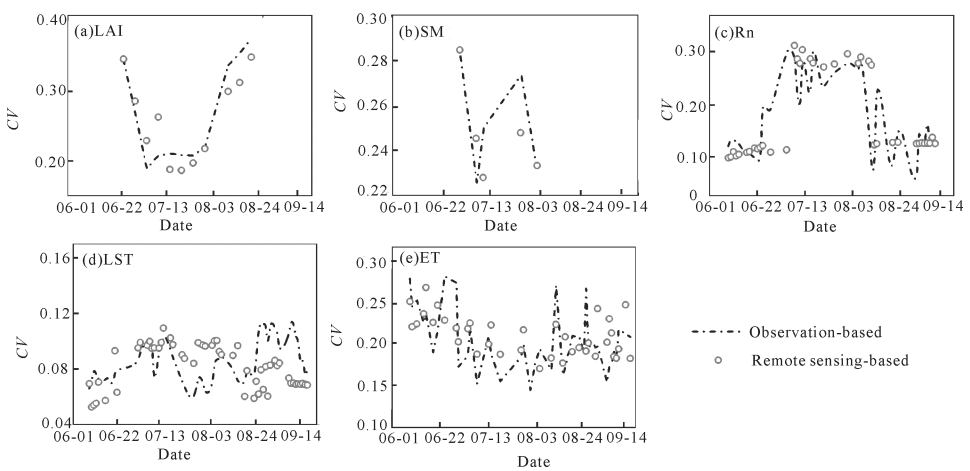

Fig. 3 Comparison of the spatial heterogeneity of LSHCs between the site measurements and remote sensing data based on the *CV* in the midstream flux observation matrix (3 km × 3 km) from June to September in 2012. LAI refers to the Leaf Area Index, SM refers to the Soil Moisture, Rn refers to the Net Radiation, LST refers to the Land Surface Temperature, and ET refers to the evapotranspiration

the spatial heterogeneity of land surface moisture conditions (Li et al., 2019; Zhang et al., 2019), thus, the SM data were not used for later analysis.

3.1.2 Comparison of evaluation methods for the LSHCs

Fig. 4 shows the spatial heterogeneity of ET during the vegetation growing season in 2012 via the midstream flux observation matrix, as described by different spatial heterogeneity evaluation indexes (*CV*, *CS*, *S′*, and *D*). The data on rainy days or in the period of irrigation were excluded. From Fig. 4, we find that except for D_{ET}, the spatial heterogeneity of ET by other evaluation indexes all present a 'U' shape, which means that those at the beginning and end of the vegetation growing season were higher, and those at the middle of the vegetation growing season were relatively lower.

The D_{ET} was unchanged throughout the entire vegetation growing season. The trend of S'_{ET} was similar to that of CS_{ET} and CV_{ET}. However, the fluctuation in S'_{ET} at the beginning and middle of the vegetation growing season was inconsistent with that in CS_{ET} and CV_{ET}. Because the S'_{ET} can describe the disorder degree of the remote sensing information, ET in the farmland tended to be more stable with the increase in crops, so S'_{ET} showed little fluctuation. While the CS_{ET} and CV_{ET} were based on the statistical method, they were vulnerable to the influence of redundancy in remote sensing data, resulting in relatively large fluctuations. Based on the above analysis, the D_{ET} was not suitable for this study area, and due to their accuracy and rationality, the other three evaluation indexes can be used to evaluate the spatial heterogeneity of LSHCs.

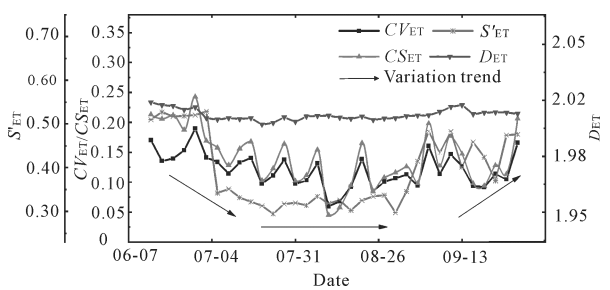

Fig. 4 Spatial heterogeneity of ET in the midstream flux observation matrix from June to September in 2012 was evaluated by the four evaluation indexes. Notes: *CV* refers to the coefficient of variation, *CS* refers to the coefficient of the sill, *S′* refers to the normalized information entropy, *D* refers to the fractal dimension, and the black arrow refers to the trend line

3.1.3 Analysis of assessment factors of the LSHCs

Based on four assessment factors (two vegetation factors, LAI and NDVI, and two energy factors, Rn and LST) and three evaluation methods (*CV*, *CS* and *S′*), the daily spatial heterogeneity was obtained. The monthly Pearson correlation coefficients between different assessment factors and ET based on three evaluation methods were shown in Table 3. The Pearson correlation coefficients can reflect the consistency between the spatial heterogeneity evaluation results based on ET and assessment factors. Each month had at least 25 d (excluding days with precipitation and irrigation).

According to Table 3, the correlation coefficients between ET and vegetation factors (LAI and NDVI) were relatively higher than ET and energy factors (Rn and LST) in the midstream flux observation matrix during the whole vegetation growing season. In the mid vegetation growing season, the Pearson correlation coefficients between Rn and ET based on evaluation methods were relatively more consistent. Since the dominant land cover type in the midstream flux observation matrix is crop, the LAI and NDVI can accurately capture the changes in vegetation phenology. The land surface characteristics changed, resulting in the uneven distribution of LSHCs and consequently influencing the spatial heterogeneity of ET. In the middle of the growing season, the crop growth tends to stabilize, so the LAI and NDVI were slightly varied. During that time, the correlation coefficients of the spatial heterogeneity between the ET and the energy factors (Rn and LST) increased. Table 3 also shows that the Pearson correlation coefficients between the four influencing factors and ET in the downstream flux observation matrix were all lower than those in the midstream matrix. Since the vegetation cover in the downstream flux observation matrix was sparse and clumped, the spatial heterogeneity of ET was more complex than that in the midstream matrix (Li et al., 2018a). In the downstream flux observation matrix, the spatial heterogeneity of LSHCs was more easily affected by vegetation factors, thus, the spatial heterogeneity described by the vegetation factors (LAI and NDVI) was consistent with ET.

As can be seen from Table 3, the performance of each evaluation method is different. In regions with relatively low spatial heterogeneity of LSHCs (such as the midstream flux observation matrix in the mid vegetation growing season), *S′* showed good performance with

Table 3 The monthly Pearson correlation coefficient of spatial heterogeneity between different assessment factors and ET based on three evaluation indexes in the midstream flux observation matrix from June to September in 2012 and downstream flux observation matrix from June to September in 2014–2015

Evaluation index	Month	Midstream matrix			Downstream matrix			
		LAI	NDVI	Rn	LST	LAI	NDVI	Rn	LST
S′	Jun.	0.60	0.64	0.41	0.38	0.47	0.46	0.09	0.15
	Jul.	0.65	0.57	0.48	0.58	0.42	0.31	0.31	0.33
	Aug.	0.63	0.46	0.59	0.31	0.35	0.45	0.33	0.37
	Sept.	0.33	0.29	0.25	0.31	0.25	0.10	0.04	0.06
	Mean	0.55	0.49	0.43	0.40	0.37	0.33	0.19	0.23
CV	Jun.	0.73	0.68	0.50	0.24	0.52	0.45	0.22	0.23
	Jul.	0.49	0.41	0.57	0.56	0.45	0.32	0.39	0.36
	Aug.	0.43	0.36	0.45	0.60	0.43	0.23	0.27	0.24
	Sept.	0.39	0.42	0.03	0.11	0.26	0.26	0.02	0.01
	Mean	0.51	0.47	0.39	0.38	0.41	0.31	0.23	0.21
CS	Jun.	0.73	0.63	0.48	0.23	0.51	0.43	0.20	0.19
	Jul.	0.52	0.44	0.55	0.54	0.44	0.28	0.41	0.29
	Aug.	0.41	0.38	0.45	0.58	0.40	0.20	0.24	0.37
	Sept.	Sept.	0.45	0.03	0.10	0.24	0.21	0.03	0.13
	Mean	Sept.	0.48	0.38	0.36	0.40	0.28	0.22	0.24

Notes: *S′*refers to the normalized information entropy, *CV* refers to the coefficient of variation, *CS* refers to the coefficient of the sill

higher Pearson coefficient. In regions with relatively high spatial heterogeneity of LSHCs (such as the downstream flux observation matrix or the midstream flux observation in the beginning and end of vegetation growing season), *CV* and *CS* displayed better performance than *S′*. According to the monthly Pearson correlation coefficients in different months, the three evaluation indexes can be complementary throughout the growing season, that is, *S′*performs well at the middle of the growing season, while *CS* and *CV* perform well at the beginning and end of the growing season. Considering that the results from the *CV* and *CS* analyses were similar and that the computational process of *CV* was simpler than that of *CS*, the *CV* was chosen. The vegetation factor showed the better performance than the energy factor, and the evaluation results of LAI and NDVI were consistent, but LAI was slightly better than NDVI based on the Pearson correlation coefficient. Thus, an evaluation scheme for the spatial heterogeneity of LSHCs was constructed by a combination of the *S′* and *CV* evaluation indexes, and the LAI was used as the assessment factor.

3.1.4 Determination of evaluation threshold of the LSHCs

Fig. 5 shows the spatial heterogeneity of the LAI and ET in the midstream and downstream flux observation matrices in the vegetation growing season. The *S′* and *CV* were used as evaluation indexes. Fig. 5a shows that when the midstream flux observation matrix was almost covered by cropland in the mid-vegetation growing season, the S'_{LAI} and S'_{ET} displayed coinciding trends, and all values were relatively small ($S'_{LAI} < 0.5$). At this time, S'_{LAI} can be used to characterize the spatial heterogeneity change of ET. However, at the beginning and end of the vegetation growing season, the spatial heterogeneity was relatively high, the S'_{LAI} was almost greater than 0.5, and the consistency between S'_{LAI} and S_{ET} was relatively low. Meanwhile, consistency of CV_{LAI} and CV_{ET} is relatively high. It indicates that CV_{LAI} can be further used to characterize the spatial heterogeneity of ET when the normalized information entropy is high (spatial heterogeneity is high). This phenomenon was rather obvious in the evaluation results of the downstream flux observation matrix (Figs. 5c and 5d). Due to the complex landscapes, the *S′* and *CV* for both the LAI and ET were much larger than those in the midstream. The S'_{LAI} was larger than 0.5, and the CV_{LAI} was larger than 0.3 for the whole vegetation growing season (Figs. 5c and 5d), and the consistency between S'_{LAI} and S'_{ET} was lower than that between CV_{LAI} and S'_{ET}. At this time, CV_{LAI} ($CV_{LAI} > 0.3$) was highly correlated with CV_{ET}, the variation trend was very consistent.

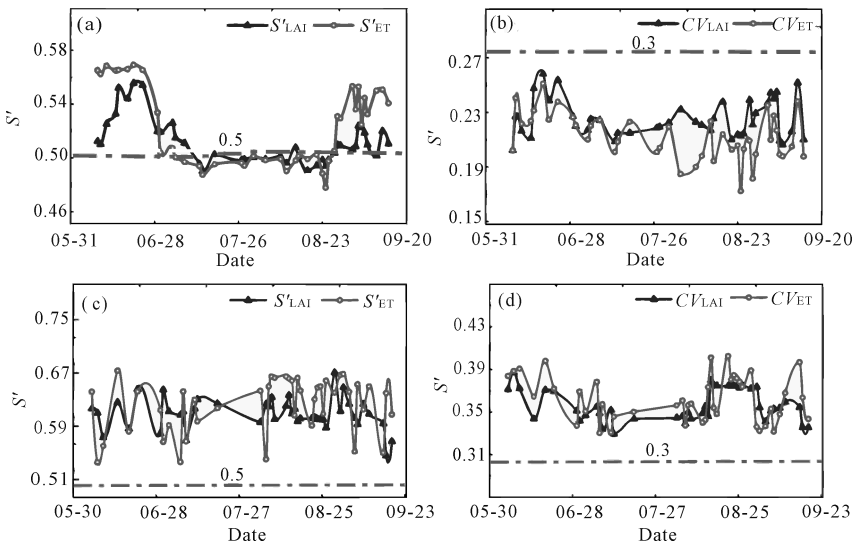

Fig. 5 The spatial heterogeneity trends between the LAI and ET for the evaluation indexes S' (a) and CV (b) in the midstream flux observation matrix (from June to September in 2012) and for indexes S' (c) and CV (d) in the downstream flux observation matrix (from June to September in 2014). S' refers to the normalized information entropy, CV refers to the coefficient of variation, the LAI refers to the Leaf Area Index, and ET refers to the evapotranspiration. The dotted line represents the threshold line in the evaluation scheme

To quantify the spatial heterogeneity of LSHCs, it is necessary to set a reasonable threshold for S'_{LAI} and CV_{LAI}. According to Fig. 5, when spatial heterogeneity is low ($S'_{LAI} < 0.5$), the spatial heterogeneity of LSHCs can be directly represented by S'_{LAI}; when spatial heterogeneity is high ($S'_{LAI} > 0.5$, while the $CV_{LAI} < 0.3$), the CV can be further used to characterize the spatial heterogeneity of LSHCs. Thus, the S'_{LAI} and CV_{LAI} thresholds can be set as 0.5 and 0.3, respectively. The spatial heterogeneity of the LSHCs can be divided into three categories. Referring to the classification of the spatial heterogeneity of LSHCs in the midstream and downstream flux observation matrices of the HRB by Li et al. (2018a), this study presents a scheme for evaluating the spatial heterogeneity of LSHCs, as shown in Table 4. The criterion to define the classification of the land surface is as follows: 1) if the S'_{LAI} is less than or equal to 0.5, it is defined as a homogeneous land surface; 2) if the S'_{LAI} is greater than 0.5, but the CV_{LAI} is less than or equal to 0.3, it is defined as a moderately heterogeneous land surface; and 3) if the S'_{LAI} is greater than 0.5 and the CV_{LAI} is greater than 0.3, it is defined as a highly heterogeneous land surface.

Table 4 Thresholds of spatial heterogeneity of LSHCs

S'LAI	CV_{LAI}	Spatial heterogeneity of LSHCs
≤0.5	≤0.3	Homogeneous
>0.5	≤0.3	Moderately heterogeneous
>0.5	>0.3	Highly heterogeneous

Notes: S'refers to the normalized information entropy, CV refers to the coefficient of variation, LAI refers to the Leaf Area Index, and LSHCs refers to the Land Surface Hydrothermal Conditions

3.2 Spatial heterogeneity of LSHCs of typical flux observation stations in the HRB

Quantitative evaluation of the LSHCs of the flux observation station is the basis for producing the ground truth ET at the pixel scale and further validating remotely sensed ET products (Li et al., 2018a). In this section, six stations with typical landscapes in the HRB were selected for evaluation. Fig. 6 shows the evaluation results (based on the 30 m remote sensing LAI data) of the spatial heterogeneity of the LSHCs at the typical flux observation stations with typical landscapes in the HRB. Based on available ground observation data and high spatial resolution remote sensing data, this study selected the upstream in 2010, midstream in 2012, and downstream in 2014 to present the evaluation results. In the upstream region, the S'_{LAI} at the Arou superstation (Fig. 6a) was less than 0.5 throughout the entire vegetation growing season and thus belonged to a relatively homogeneous land surface. The Guantan station (Fig. 6b) was moderately heterogeneous in the early and late

growing seasons ($S'_{LAI} > 0.5$ and $CV_{LAI} < 0.3$), while it tended to be homogeneous in the middle of the growing season ($S'_{LAI} < 0.5$). The spatial heterogeneity of the LSHCs at the Daman superstation (Fig. 6c) in the midstream region was consistent with that at the Guantan station, but the CV_{LAI} and S'_{LAI} were relatively lower than those at the Guantan station. The S'_{LAI} for the Zhangye wetland station (Fig. 6d) in the growing season was greater than 0.5, and the CV_{LAI} was lower than 0.3, so this station was moderately heterogeneous. The spatial heterogeneity of LSHCs at the downstream mixed forest station (Fig. 6e) displayed two states of spatial heterogeneity in the vegetation growing season: the S'_{LAI} was greater than 0.5, and the CV_{LAI} was lower than 0.3 at the end of July and August, making this region belong to the moderately heterogeneous land surface. In other months, the S'_{LAI} and CV_{LAI} were greater than their respective thresholds, so the region belonged to the highly heterogeneous land surface. In downstream areas, the S'_{LAI} and CV_{LAI} of the Sidaoqiao superstation (Fig. 6f) were greater than 0.5 and 0.3 in the whole growing season, respectively, thus, this region was highly heterogeneous.

The Google Earth imagery (Fig. 7) and remotely sensed ET data with high spatial-temporal resolution (Fig. 8) were used to validate the evaluation results of the spatial heterogeneity of LSHCs. Fig. 8 shows that the spatial heterogeneity of the ET in the Arou superstation upstream was much lower than that of the other stations. The Arou superstation was on the meadow land surface (Fig. 7a), and the spatial distribution difference in ET during the growing season was the smallest. At Daman superstation (Fig. 8), the spatial heterogeneity described by ET was small in the middle of the growing season and large in the early and late stages of the growing season. The Daman superstation was mainly covered by farmland (Fig. 7c), and vegetation grew rapidly in the early growing season. In the late growing season, vegetation gradually withered. ET changed greatly in these two periods, which led to higher spatial heterogeneity of ET. The distribution of ET tended to be consistent; the spatial heterogeneity of ET decreased in

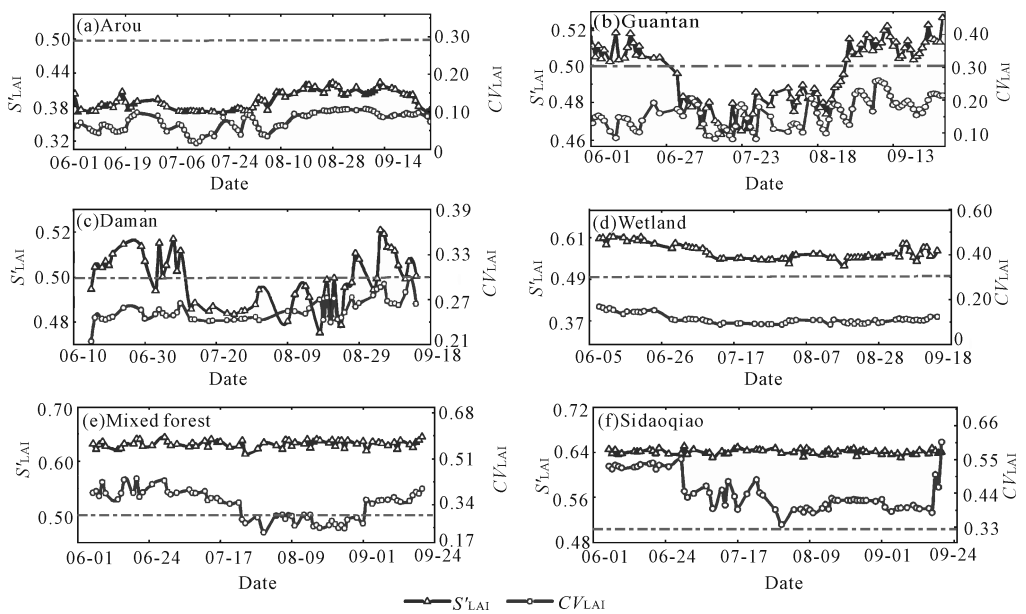

Fig. 6 The spatial heterogeneity of LSHCs in the vegetation growing season of typical flux observation stations in the HRB. (a) is the Arou superstation in 2010, (b) is the Guantan station in 2010, (c) is the Daman superstation in 2012, (d) is the Zhangye wetland station in 2012, (e) is the Mixed forest station in 2014, and (f) is the Sidaoqiao superstation in 2014. The dotted line represents the threshold line in the evaluation scheme. *S'* refers to the normalized information entropy, *CV* refers to the coefficient of variation, and LAI refers to the Leaf Area Index

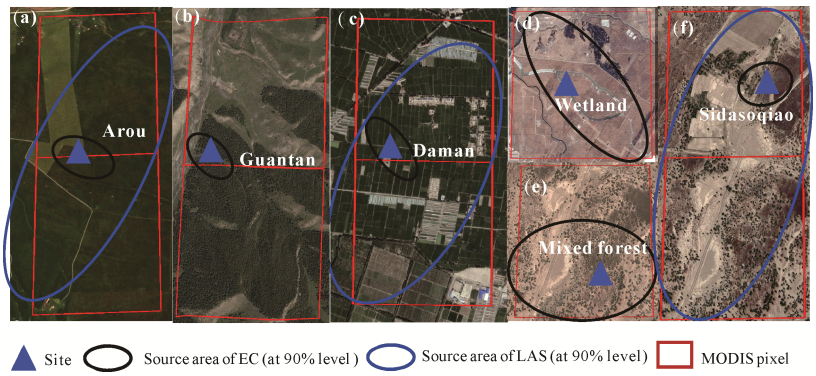

Fig. 7 The spatial heterogeneity of LSHCs based on the Google Earth imagery of MODIS pixels covered byfootprint at the (a) Arou superstation, (b) Guantan station (c) Daman superstation, (d) Zhangye Wetland station, (e) Mixed forest station, and (f) Sidaoqiao superstation. EC refers to the eddy covariances system, LAS refers to the large aperture scintillator and MODIS refers to the Moderate Resolution Imaging Spectroradiometer

the middle of the growing season. The spatial heterogeneity of ET at Guantan station was similar to that at the Daman superstation, but the S'_{ET} was relatively higher than that at the Daman superstation. The land cover at Guantan station was mixed with evergreen coniferous forest *Picea crassifolia* and meadow (Fig. 7b). With the further coverage of meadows in the middle of the growing season, the spatial heterogeneity of ET tended to decrease, so the curve of S'_{ET} trended down and then increased toward the end of the growing season. The wetland station was located in Zhangye National Wetland Park (Fig. 7d). The land surface had a staggered distribution of reeds, ditches, water bodies, etc. Because of the uneven distribution of moisture and vegetation, the spatial distribution of ET was always higher than that at the Daman superstation, and the Zhangye wetland station belonged to the moderately heterogeneous land surface. The high S'_{ET} was related to the fragmented landscape. The farmland, bare land, sparse tamarisk, and *Populus euphratica* were scattered in the downstream (Figs. 7e and 7f), and the climate was dry, which made the differences in the spatial distribution of SM and groundwater obviously and further increased in the spatial heterogeneity of ET. The mixed forest station had relatively low spatial heterogeneity in late July and August. In other months, the spatial heterogeneity of ET was high, and Sidaoqiao superstation had high spatial heterogeneity of ET for the whole vegetation growing season (Fig. 8).

The spatial heterogeneity of the LSHCs for the six stations from the HRB was evaluated based on the evaluation scheme. The evaluation results were validated by

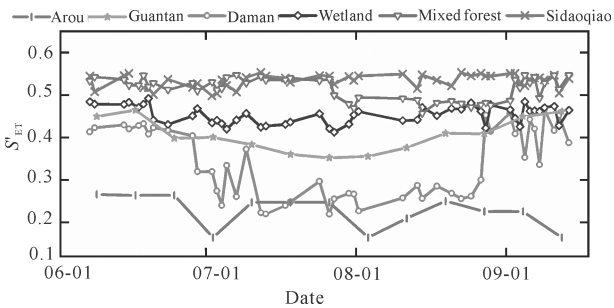

Fig. 8 The spatial heterogeneity assessment results in vegetation growing season based on S'_{ET} (the evaluation results of Arou superstation and Guantan station in upstream were in 2010, the evaluation results of Daman superstation and Wetland station in midstream were in 2012, and the evaluation results of Sidaoqiao superstation and Mixed forest station in downstream were in 2014). S' refers to the normalized information entropy, ET refers to the evapotranspiration

Google Earth imagery and high spatial-temporal resolution remotely sensed ET, which indicated that the evaluation results were accurate and that the evaluation scheme proposed in this study was reasonable.

4 Impact factors analysis of spatial heterogeneity evaluation

4.1 Impact of precipitation and irrigation events

Fig. 9 displays the change in the spatial heterogeneity of the LSHCs during irrigation and precipitation events in the midstream flux observation matrix. The high spatial-temporal resolution remotely sensed ET was used as the reference. Because remotely sensed LST data were lacking under precipitation and irrigation conditions, the LAI and Rn were used as vegetation factors and energy

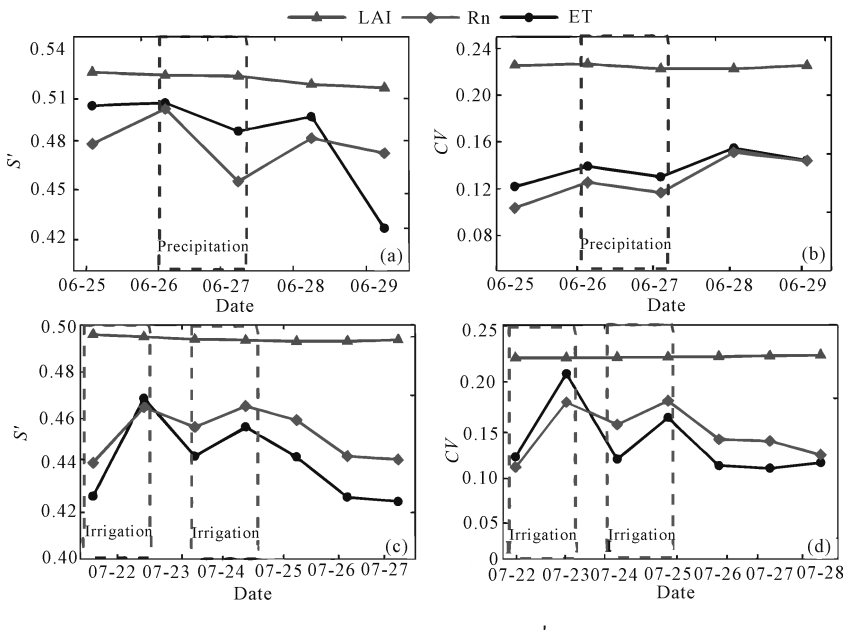

Fig. 9 Effects of precipitation and irrigation events on the evaluation results of the spatial heterogeneity of LSHCs in midstream flux observation matrix. The evaluation results were based on *S*′ (a) and *CV* (b) during the rainfall events (2012-06-25 to 2012-06-29) and based on *S*′(c) and *CV* (d) during the irrigation events (2012-07-22 to 2012-07-28). *S*′ refers to the normalized information entropy, CV refers to the coefficient of variation, LAI refers to the Leaf Area Index, Rn refers to the Net Radiation, ET refers to the evapotranspiration

factors, respectively. The precipitation events occurred on June 26 and June 27 in 2012. After precipitation, the LSHCs became uniform. In Figs. 9a and 9b, the spatial heterogeneity of the ET described by *S*′and *CV* decreased. The spatial heterogeneity reflected by Rn displayed a consistent trend with ET. However, this change of spatial heterogeneity of LSHCs during the precipitation event was hardly captured by the LAI. Similar to the precipitation events, the irrigation events occurred on July 22 and 24, which caused the change in spatial heterogeneity of LSHCs. In the early stage of irrigation, some farmlands were irrigated, while others were not. As a result, the SM in irrigated farmland increased significantly, which increased the ET. In nonirrigated farmland, the ET was unchanged, which resulted in a larger spatial distribution difference in ET and increased spatial heterogeneity of LSHCs regionally. Under the conditions of irrigation, the vegetation factor (LAI) was basically unresponsive to irrigation processes, while the energy factor still had a relatively consistent trend with ET. In conclusion, the energy factor can reflect and capture the short-term rapid change process (such as rainfall and irrigation) of the spatial heterogeneity of LSHCs. In contrast, the vegetation factor can depict the long-term gradual change process in the spatial heterogeneity of LSHCs but can not immediately reflect rapid changes.

4.2 Impact of different spatial resolutions of remote sensing data and heterogeneity in the vertical direction

The spatial resolutions of remote sensing data from different satellites or airborne sensors may be significantly different. A surface parameter that is homogeneous at one spatial resolution may tend to be heterogeneous at other spatial resolutions. Therefore, the effect of different spatial resolutions in remote sensing data should be analyzed. In this section, the spatial heterogeneities of the LAI and LST described by *S*′ and *CV* were compared based on airborne and satellite remote sensing data at different spatial resolutions. As the spatial resolution decreased, the detailed information reflected by higher spatial resolution remote sensing images was lost, resulting in a reduction in the spatial heterogeneity of LSHCs.

Fig. 10 also shows that at spatial resolutions of 30 m

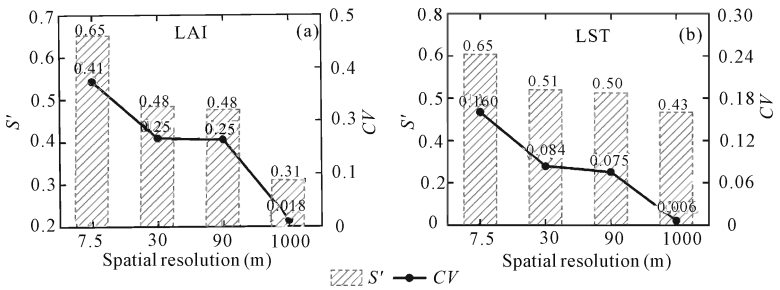

Fig. 10 The effect of the remotely sensed (a) LAI and (b) LST at different spatial resolutions on the evaluation results in midstream flux observation matrix on August 2, 2012. *S*' refers to the normalized information entropy, *CV* refers to the coefficient of variation, LAI refers to the Leaf Area Index, and LST refers to the Land Surface Temperature

and 90 m, the evaluation schemes have little influence on the evaluation results. However, when using data with a 7.5 m or 1000 m spatial resolution, the corresponding spatial heterogeneity obviously exceeds or falls below the threshold of the proposed spatial heterogeneity evaluation scheme, which has a great influence on the evaluation results of spatial heterogeneity. The evaluation scheme in this study was based on data with a 30 m spatial resolution. When there are remote sensing data with higher (meter level) or lower (kilometer level) spatial resolutions, the settings of the threshold values should be different.

Generally, optical remote sensing data can obtain information in the horizontal direction rather than in the vertical direction(Li and Reynolds, 1995). Therefore, there are relatively few studies on the effect of vertical heterogeneity on horizontal spatial heterogeneity. There were not only crops, vegetation, and maize but also some orchard and shelterbelts in the midstream flux observation matrix. In the downstream flux observation matrix, in addition to farmland, there were also scattered *Tamarix* and *Populus euphratica* vegetation types. The various vegetation types with different heights may affect the spatial heterogeneity of the LSHCs. Active remote sensing data, such as Lidar, can describe the vertical structure of the land surface; thus, based on the Leaf Area Density (LAD) data (Liu et al., 2018a) obtained by Lidar in the midstream and downstream flux observation matrixes, this study discussed the influence of LAD at different vertical levels on the spatial heterogeneity of LSHCs in the horizontal direction. The LAD used in this study refers to the total leaf area per unit community volume, and the LAI (z) is the integrated LAD at a corresponding height of *z*. From Fig. 11, the heterogeneity of LAD in the vertical direction significantly affects the spatial heterogeneity of the LAI in the horizontal direction, which showed a positive correlation. In the midstream observation flux matrix (Fig. 11a), the CV-LAD displayed a three-layer spatial heterogeneity structure (I, II, and III in Fig. 11a) in the vertical direction, with heights ranging from 0 to 2 m, 2 to 5 m and 5 to 30 m. The layers coincided with the heights of farmland (maize), village and shelterbelt covers. When the heights exceeded 5 m (III), the spatial heterogeneity of the LAI in the horizontal direction tended to stabilize and did not change with the heterogeneity of LAD in the vertical direction. The CV-LAD changed rapidly in the downstream flux observation matrix because there were mainly low farmland (such as melon crops), tamarisk and tall poplar forests. Therefore, the spatial heterogeneity of LAD in the vertical direction changed rapidly, but the spatial heterogeneity of the LAI in the horizontal direction tended to be stable after a 4 m height.

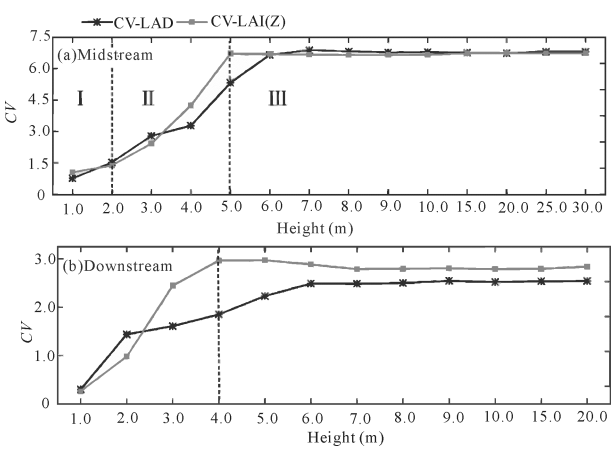

Fig. 11 Effects of vertical heterogeneity on horizontal spatial heterogeneity in the midstream (July 19, 2012) (a) and downstream regions (July 29, 2014) (b) of the HRB. *CV* refers to the coefficient of variation, LAI refers to the Leaf Area Index, and LAD refers to the Leaf Area Density. The dotted line indicates that the spatial heterogeneity of LSHCs appears obvious change at 2 m, 4 m and 5 m

In conclusion, the heterogeneity of vegetation in the vertical direction can affect the spatial heterogeneity in the horizontal direction. When the vegetation distribution exceeds a certain height, the spatial heterogeneity in the horizontal direction would not change significantly because of reduced vegetation distribution. Therefore, the vertical heterogeneity of vegetation should be taken into account when evaluating the spatial heterogeneity of LSHCs under different vegetation height conditions.

4.3 Impact of topography and sparse vegetation

The influence of topography and low vegetation cover on the evaluation result should also be analyzed. The terrain in the midstream and downstream regions of the HRB is relatively flat, but that in the upstream region is in high-altitude, mountainous areas with complex topography. The MODIS pixels corresponding to flux observation stations may have large topographic relief in the upstream, such as at Yakou station, Huludou station, and Jingyangling station. The altitudes of the three stations exceeded 3200 m, and that of the Yakou station was even at 4149 m. Complex terrain can bring a challenge to accurately evaluate the heterogeneity of LSHCs. Therefore, based on the slope map and Google imagery map, the evaluation results of the spatial heterogeneity of LSHCs affected by topography were analyzed. The evaluation results of the spatial heterogeneity of LSHCs are shown in Fig. 12. The S'_{LAI} of these stations was lower than 0.5, and the CV_{LAI} was lower than 0.3, so these were determined to belong to a homogeneous land surface. However, from slope maps and Google Earth imagery maps (Fig. 13), these stations were located on the hillside, with a rolling topography, and the pathway, meadow, and shrub land types were distributed within the MODIS pixels. The maximum change in Digital Elevation Model (DEM) in these stations can reach 280 m; the maximum change in slope can reach 45°. Changes in elevation and slope can affect the distributions of temperature, moisture, and other environmental factors to form local heterogeneity. The spatial heterogeneity of these stations should not be homogeneous. Because the influence of terrain factors on the spatial heterogeneity of LSHCs was not taken into account in the evaluation scheme, the evaluation results deviated from reality.

Topography has an important influence on the evaluation results of the spatial heterogeneity of LSHCs. The evaluation scheme proposed in this study was mainly aimed at a flat terrain area and did not consider the impact of topographic rolling, so the scheme may not be suitable for flux observation stations on undulating terrains.

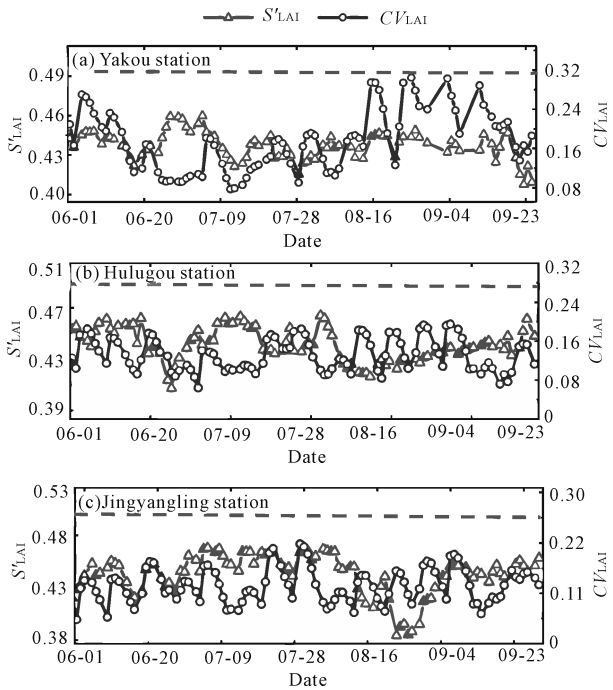

Fig. 12 Evaluation results of the spatial heterogeneity of LSHCs for (a) Yakou station, (b) Hulugou station and (c) Jingyangling station from June to September in 2010. S' refers to the normalized information entropy, CV refers to the coefficient of variation, LAI refers to the Leaf Area Index. The dotted line represents the threshold line in the evaluation scheme

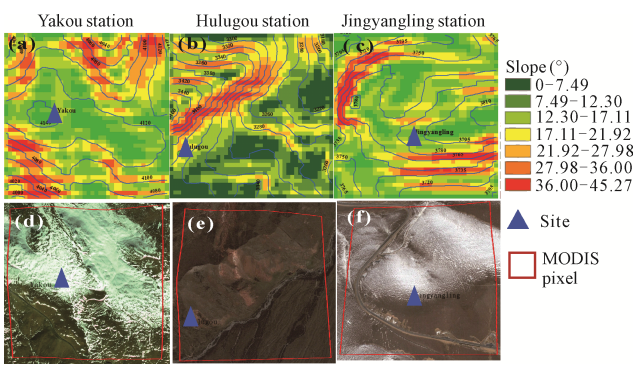

Fig. 13 Slope map for (a) Yakou station, (b) Hulugou station, (c) Jingyangling station and the Google Earth imagery for (d) Yakou station, (e) Hulugou station and (f) Jingyangling station. MODIS refers to the Moderate Resolution Imaging Spectroradiometer

This evaluation scheme constructed in this study was based on LAI and has been validated in relatively dense vegetation stations. However, the impact of low vegetation cover on the spatial heterogeneity evaluation of LSHCs is still lacking. Therefore, this study selected four stations (Bajitan, ShenShawo, Huazhaizi, and Desert) with low vegetation cover to evaluate and analyze the spatial heterogeneity of LSHCs. The evaluation results were validated by remotely sensed ET at a high spatial resolution. The evaluation results are shown in Fig. 14a. The downstream desert station was moderately heterogeneous, and the Bajitan, Shenshawo, and Huazhaizi station in the midstream were homogeneous. From the validation results of ET in Fig. 14b, the desert station should be homogeneous because the mean S'_{ET} at this station was lower than 0.2. The validation results of Bajitan station, Shenshawo station, and Huazhaizi station were consistent with those of the evaluation result. However, the discrepancy between the S'_{ET} and S'_{LAI} of ShenShawo was relatively large, which may be because the distribution of the LAI was more complex and severely uneven at this station. At the desert station, the evaluation results from ET and LAI were inconsistent, which may be due to the low vegetation cover. The average LAI at this station was approximately 0.25, which was the lowest at these four stations. Therefore, using a vegetation factor (LAI) to evaluate the spatial heterogeneity of LSHCs may bring differences in sparse vegetation areas. The evaluation scheme in this study was not suitable for flux observation stations with sparse vegetation cover.

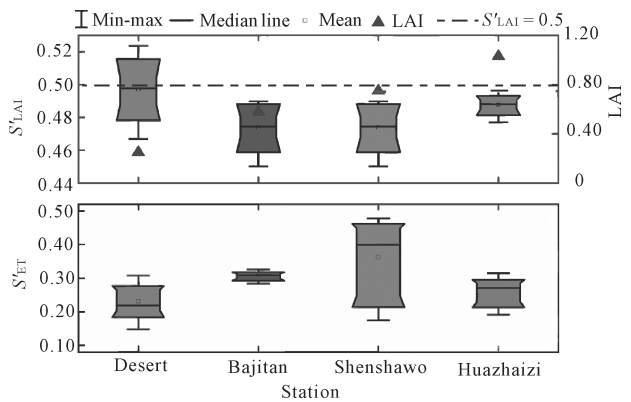

Fig. 14 Effects of low vegetation cover on the spatial heterogeneity evaluation of LSHCs based on (a) LAI and (b) ET (The S'_{LAI} and S'_{ET} of Bajitan station, Shenshawo station and Huazhaizi station were from June to September in 2012, of Desert station was from June to September in 2015). S' refers to the normalized information entropy, ET refers to the evapotranspiration, and LAI refers to the Leaf Area Index

5 Conclusions

Accurately evaluating the spatial heterogeneity of LSHCs at different flux observation stations can improve the accuracy of validation of the remotely sensed (or model simulated) ET. This study was based on observation data from the HiWATER-MUSOEXE experiment and the Heihe integrated observatory, with high-resolution satellite and airborne remote sensing data to construct an evaluation scheme for the spatial heterogeneity of LSHCs. The typical flux observation stations in the HRB was evaluated, and the evaluation results were validated. Moreover, this study discussed the effects of some impact factors for the evaluation result. The main conclusions are as follows:

1) Based on the coefficient of variation (*CV*), high spatial resolution remote sensing data such as the LAI, LST, Rn, and ET were consistent with the on-site measurement data indicated that the high spatial resolution remote sensing data can be used to evaluate the spatial heterogeneity. However, the spatial resolution of remote sensing SM data inverted by PLMR was too coarse (700 m), so it hard to reflect the change of spatial heterogeneity at the field scale.

2) After the selection of evaluation methods and assessment factors, this evaluation scheme for the spatial heterogeneity of LSHCs was based on a 30 m resolution LAI and the evaluation indexes *CV* and S'. If the S'_{LAI} was less than or equal to 0.5, the land surface was defined as homogeneous. If the S'_{LAI} was greater than 0.5 and the CV_{LAI} was less than or equal to 0.3, the land surface was defined as moderately heterogeneous. If the S'_{LAI} was greater than 0.5 and the CV_{LAI} was greater than 0.3, the land surface was defined as highly heterogeneous.

3) The evaluation results from typical land surface stations showed that different stations have different spatial heterogeneities of LSHCs. For example, the Arou superstation was homogeneous throughout the growing season, and the Daman superstation in the middle of the growing season was homogeneous, but moderately heterogeneous before and after the growing season. The Sidaoqiao superstation was highly heterogeneous. The evaluation results of stations were validated by the remotely sensed ET data and Google Earth imagery.

4) The impact factors for the evaluation result were also analyzed. The short-term rapid change process in

the spatial heterogeneity of LSHCs can be reflected by energy factors, while the long-term change can be reflected by vegetation factors. The spatial heterogeneity of LSHCs decreases as the spatial resolution of remote sensing data decreases. The spatial heterogeneity in the horizontal direction can be affected by the heterogeneity in the vertical direction. The flux observation stations with substantial terrain or excessively sparse vegetation were not suitable for the evaluation scheme, due to the influences of terrain and vegetation density were not considered.

The spatial heterogeneity of the LSHCs evaluation scheme was constructed by commonly used spatial heterogeneity evaluation indexes. By improving the understanding of spatial heterogeneity, other spatial heterogeneity evaluation indexes such as the characteristic scale (used in wavelet analysis method could be introduced in subsequent research. The threshold of the spatial heterogeneity evaluation scheme constructed in this study was based on the evaluation results of the midstream and downstream flux observation matrixes of the HRB. For different spatial resolution remote sensing data, the threshold of the evaluation scheme may be different, which needs to be considered in future work. In this study, the effects of precipitation and irrigation events, vertical spatial heterogeneity, topography and vegetation density on the evaluation of the spatial heterogeneity of LSHCs were discussed. Corresponding solutions should be proposed in the future. In addition, the results of heterogeneity evaluation need to be extended to the whole year to provide a basis for better analyzing seasonal and interannual variations of the spatial heterogeneity of LSHCs.

Acknowledgment

We would like to thank all the scientists, engineers, and students who participated in HiWATER field campaigns.

References

Alfieri J G, Niyogi D, Zhang H et al., 2009. Quantifying the spatial variability of surface fluxes using data from the 2002 International H2O Project. *Boundary-Layer Meteorology,* 133(3): 323. doi: 10.1007/s10546-009-9406-2

Bhattacharya B K, Mallick K, Patel N K et al. 2010. Regional clear sky evapotranspiration over agricultural land using remote sensing data from Indian geostationary meteorological satellite. *Journal of Hydrology*, 387(1–2): 65–80. doi: 10.1016/j.jhydrol.2010.03.030

Boudreault L-É, Bechmann A, Tarvainen L et al., 2015. A LiDAR method of canopy structure retrieval for wind modeling of heterogeneous forests. *Agricultural Forest Meteorology,* 201: 86–97. doi: 10.1016/j.agrformet.2014.10.014

Clarke K C. 1986. Computation of the fractal dimension of topographic surfaces using the triangular prism surface area method. *Computers & Geosciences*, 12(5): 713–722. doi: 10.1016/0098-3004(86)90047-6

Cressie N, Zimmerman D L, 1992. On the stability of the geostatistical method. *Mathematical Geology*, 24(1): 45–59

Chen R S, Song Y X, Kang E S et al., 2014. A cryosphere-hydrology observation system in a small alpine watershed in the Qilian Mountains of China and its meteorological gradient. *Arctic Antarctic Alpine Research,* 46(2): 505–523. doi: 10.1657/1938-4246-46.2.505

Ding Y, Zhao K, Zheng X et al., 2014. Temporal dynamics of spatial heterogeneity over cropland quantified by time-series NDVI, near infrared and red reflectance of Landsat 8 OLI imagery. *International Journal of Applied Earth Observation Geoinformation*, 30: 139–145.doi: 10.1016/j.jag.2014.01.009

Gao G, Chen D, Ren G et al., 2006. Spatial and temporal variations and controlling factors of potential evapotranspiration in China: 1956–2000. *Journal of Geographical Sciences,* 16(1): 3–12. doi: 10.1007/s11442-006-0101-7

Gao J, Wu S, Dai E F et al., 2015. The progresses and prospects of research on water and heat balance at land surface in the Karst region of Southwest China. *Advances in Earth Science,* 30(6): 647–653. doi: 10.11867/j.issn.1001-8166.2015.06.0647

Garrigues S, Allard D, Baret F et al., 2006. Quantifying spatial heterogeneity at the landscape scale using variogram models. *Remote Sensing of Environment,* 103(1): 81–96. doi: 10.1016/j.rse.2006.03.013

Ge Y, Jin Y, Stein A et al., 2019. Principles and methods of scaling geospatial Earth science data. *Earth-Science Reviews*: 102897. doi: 10.1016/j.earscirev.2019.102897

Giannico V, Chen J, Shao C et al., 2018. Contributions of landscape heterogeneity within the footprint of eddy-covariance towers to flux measurements. *Agricultural Forest Meteorology,* 260: 144–153. doi: 10.1016/j.agrformet.2018.06.004

Han D, Wang G, Liu T et al., 2018. Hydroclimatic response of evapotranspiration partitioning to prolonged droughts in semiarid grassland. *Journal of Hydrology*, 563: 766–777. doi: 10.1016/j.jhydrol.2018.06.048

Hu T, Liu Q, Du Y et al., 2015. Analysis of land surface temperature spatial heterogeneity using variogram model. Paper presented at the *2015 IEEE International Geoscience and Remote Sensing Symposium* (IGARSS). doi: 10.1109/IGARSS.2015.7325716

Jia Z, Liu S, Xu Z et al., 2012. Validation of remotely sensed evapotranspiration over the Hai River Basin, China. *Journal of Geophysical Research: Atmospheres,* 117(D13). doi: 10.1029/2011JD017037

Jin R, Li X, Yan B et al., 2014. A nested ecohydrological wireless

sensor network for capturing the surface heterogeneity in the midstream areas of the Heihe River Basin, China. *IEEE Geoscience Remote Sensing Letters,* 11(11): 2015–2019. doi: 10.1109/lgrs.2014.2319085

Kormann R, Meixner F X, 2001. An analytical footprint model for non-neutral stratification. *Boundary*: *Layer Meteorology,* 99(2): 207–224. doi: 10.1023/a:1018991015119

Kong J, Hu Y, Yang L et al., 2019. Estimation of evapotranspiration for the blown-sand region in the Ordos basin based on the SEBAL model. *International Journal of Remote Sensing*, 40(5–6): 1945–1965. doi: 10.1080/01431161.2018.1508919

Li Band Avissar R, 1994. The impact of spatial variability of land-surface characteristics on land-surface heat fluxes. *Journal of Climate,* 7(4): 527–537. doi: 10.1175/1520–0442(1994)007<0527:tiosvo>2.0.co;2

Li Hand Reynolds J, 1995. On definition and quantification of heterogeneity. *Oikos*: 280–284. doi: 10.2307/3545921

Li M, Zhou J, Peng Z et al., 2019. Component radiative temperatures over sparsely vegetated surfaces and their potential for upscaling land surface temperature. *Agricultural Forest Meteorology,* 276: 107600. doi: 10.1016/j.agrformet.2019.05.031

Li X, Li X, Li Z et al., 2009. Watershed allied telemetry experimental research. *Journal of Geophysical Research: Atmospheres,* 114(D22): 2191–2196. doi: 10.1029/2008JD011590

Li X, Cheng G, Liu S et al., 2013. Heihe watershed allied telemetry experimental research (HiWATER): scientific objectives and experimental design. *Bulletin of the American Meteorological Society,* 94(8): 1145–1160. doi: 10.1175/BAMS-D-12-00154.1

Li X, Liu S, Li H et al., 2018a. Intercomparison of six upscaling evapotranspiration methods: from site to the satellite pixel. *Journal of Geophysical Research: Atmospheres,* 123(13): 6777–6803. doi: 10.1029/2018JD028422

Li X, Liu S, Xiao Q et al., 2017. A multiscale dataset for understanding complex eco-hydrological processes in a heterogeneous oasis system. *Scientific Data,* 4: 170083. doi: 10.1038/sdata.2017.83

Li X, Xin X, Peng Z et al., 2018b. Analysis of the spatial variability of land surface variables for ET estimation: case study in HiWATER Campaign. *Remote Sensing,* 10(1): 91. doi: 10.3390/rs12010010091

Liu R, Liu S, Yang X et al., 2018a. Wind dynamics over a highly heterogeneous oasis area: an experimental and numerical study. *Journal of Geophysical Research: Atmospheres,* 123(16): 8418–8440. doi: 10.1029/2018JD028397

Liu S, Xu Z, Wang W et al., 2011. A comparison of eddy-covariance and large aperture scintillometer measurements with respect to the energy balance closure problem. *Hydrology Earth System Sciences,* 15(4): 1291–1306. doi: 10.5194/hess-15-1291-2011

Liu S, Xu Z, Song L et al., 2016. Upscaling evapotranspiration measurements from multi-site to the satellite pixel scale over heterogeneous land surfaces. *Agricultural and Forest Meteorology,* 230–231: 97–113. doi: 10.1016/j.agrformet.2016.04.008

Liu S, Li X, Xu Z et al., 2018b. The Heihe integrated observatory network: a basin-scale land surface processes observatory in China. *Vadose Zone Journal,* 17(1). doi: 10.2136/vzj2018.04.0072

Ma Y, Liu S, Song L et al., 2018. Estimation of daily evapotranspiration and irrigation water efficiency at a Landsat-like scale for an arid irrigation area using multi-source remote sensing data. *Remote Sensing of Environment,* 216: 715–734. doi: 10.1016/j.rse.2018.07.019

Ma Y, Li X, Liu L et al., 2019. Evapotranspiration and its dominant controls along an elevation gradient in the Qinghai Lake watershed, northeast Qinghai-Tibet Plateau. *Journal of Hydrology*, 575: 257–268. doi: 10.1016/j.jhydrol.2019.05.019

Matheron G, 1963. Principles of geostatistics. *Economic geology,* 58(8): 1246–1266

Meijninger W, Hartogensis O, Kohsiek W et al., 2002. Determination of area-averaged sensible heat fluxes with a large aperture scintillometer over a heterogeneous surface-Flevoland field experiment. *Boundary*: *Layer Meteorology,* 105(1): 37–62. doi: 10.1023/A:1019647732027

Nakayama T. 2013. Effect of evapotranspiration on hydrothermal changes in regional scale. In: *Evapotranspiration: An Overview*. doi: 10.5772/52808. Available at: https://www.intechopen.com/books/evapotranspiration an overview/effect of evapotranspiration on hydrothermal changes in regional scale

Odongo V, Hamm Nand Milton E, 2014. Spatio-temporal assessment of Tuz Gölü, Turkey as a potential radiometric vicarious calibration site. *Remote Sensing,* 6(3): 2494–2513. doi: 10.3390/rs6032494

Qu Y, Zhu Y, Han W et al., 2013. Crop leaf area index observations with a wireless sensor network and its potential for validating remote sensing products. *IEEE Journal of Selected Topics in Applied Earth Observations Remote Sensing,* 7(2): 431–444. doi: 10.1109/JSTARS.2013.2289931

Shannon C E, 1948. A mathematical theory of communication. *Bell System Technical Journal,* 27(3): 379–423. doi: 10.1002/j.1538-7305.1948.tb01338.x

Sun W, Xu G, Gong P et al., 2006. Fractal analysis of remotely sensed images: a review of methods and applications. *International Journal of Remote Sensing,* 27(22): 4963–4990. doi: 10.1080/01431160600676695

Twine T E, Kustas W, Norman J et al., 2000. Correcting eddy-covariance flux underestimates over a grassland. *Agricultural Forest Meteorology,* 103(3): 279–300. doi: 10.1016/S0168-1923(00)00123-4

Wang J, Ge Y, Heuvelink G B et al., 2013. Spatial sampling design for estimating regional GPP with spatial heterogeneities. *IEEE Geoscience Remote Sensing Letters,* 11(2): 539–543. doi: 10.1109/LGRS.2013.2274453

Wang J, Zhang Tand Fu B,2016. A measure of spatial stratified heterogeneity. *Ecological Indicators,* 67: 250–256. doi: 10.1016/j.ecolind.2016.02.052

Wang Z, Wu Q, Fan B, et al. 2019. Effects of mulching biodegradable films under drip irrigation on soil hydrothermal conditions and cotton (*Gossypium hirsutum* L.) yield. *Agricultural*

water management, 213: 477–485. doi: 10.1016/j.agwat.2018.10.036

Wu X, Xiao Q, Wen J, et al., 2019. Advances in quantitative remote sensing product validation: overview and current status. Earth-Science Reviews, 102875. doi: 10.1016/j.earscirev.2019.102875

Xiao Q, Wen J, 2013. HiWATER: Wide-angle infrared dual-mode line/area array scanner, WIDAS (3th, August, 2012). *Heihe Plan Science Data Center, Heihe, China.* Datasets available at: http://westdc.westgis.ac.cn

Xu B, Li J, Liu Q et al., 2016. Evaluating spatial representativeness of station observations for remotely sensed leaf area index products. *IEEE Journal of Selected Topics in Applied Earth Observations Remote Sensing,* 9(7): 3267–3282. doi: 10.1109/JSTARS.2016.2560878

Xu T, Guo Z, Liu S et al., 2018. Evaluating different machine learning methods for upscaling evapotranspiration from flux towers to the regional scale. *Journal of Geophysical Research: Atmospheres,* 123(16): 8674–8690. doi: 10.1029/2018JD028447

Xu T, He X, Bateni S M et al., 2019. Mapping regional turbulent heat fluxes via variational assimilation of land surface temperature data from polar orbiting satellites. *Remote Sensing of Environment,* 221: 444–461. doi: 10.1016/j.rse.2018.11.023

Xu Z, Liu S, Li X et al., 2013. Intercomparison of surface energy flux measurement systems used during the HiWATER-MUSOEXE. *Journal of Geophysical Research: Atmospheres,* 118(23): 13,140–113,157. doi: 10.1002/2013JD 020260

Zhang K, Kimball J S, and Running S W. 2016. A review of remote sensing based actual evapotranspiration estimation. *Wiley Interdisciplinary Reviews: Water*, 3(6): 834–853. doi: 10.1002/wat2.1168

Zhang X, Zhou J, Göttsche F M et al., 2019. A method based on temporal component decomposition for estimating 1-km all-weather land surface temperature by merging satellite thermal infrared and passive microwave observations. *IEEE Transactions on Geoscience Remote Sensing*, 57(7): 4670–4691. doi: 10.1109/TGRS.2019.2892417

Zhu X, Chen J, Gao F et al., 2010. An enhanced spatial and temporal adaptive reflectance fusion model for complex heterogeneous regions. *Remote Sensing of Environment,* 114(11): 2610–2623. doi: 10.1016/j.rse.2010.05.032

Zhong B, Ma P, Nie A H et al., 2014. Land cover mapping using time series HJ-1/CCD data. *Science China Earth Sciences*, 57(8): 1790–1799. doi: 10.1007/s11430-014-4877-5